Renner–Teller induced predissociation of HNO (Ã 1 A ″): Rotational-state dependent linewidths of quasibound states

Jan Weiß and Reinhard Schinke

Citation: The Journal of Chemical Physics **115**, 3173 (2001); doi: 10.1063/1.1384456
View online: http://dx.doi.org/10.1063/1.1384456
View Table of Contents: http://scitation.aip.org/content/aip/journal/jcp/115/7?ver=pdfcov
Published by the AIP Publishing

Renner–Teller induced predissociation of HNO($\tilde{A}\,^1A''$): Rotational-state dependent linewidths of quasibound states

Jan Weiß and Reinhard Schinke
Max-Planck-Institut für Strömungsforschung, D-37073 Göttingen, Germany

(Received 16 April 2001; accepted 17 May 2001)

The predissociation dynamics in the $\tilde{A}\,^1A''$ electronic state of HNO is investigated. The quantum mechanical dynamics calculations take into account the Renner–Teller (or electronic Coriolis) coupling with the electronic ground state $\tilde{X}\,^1A'$, which appears to be the dominant decay mechanism for the quasi-bound vibrational states in the $\tilde{A}\,^1A''$ upper state. All three internal vibrational degrees of freedom are incorporated and two *ab initio* potential energy surfaces are used. The linewidths, Γ, are directly calculated by the filter diagonalization method and an absorbing optical potential in the exit channel. They are generally small ($\sim 1\,\mathrm{cm}^{-1}$) and increase with excitation of the bending mode (bent-to-bent transition). On average, Γ increases with K, the a-axis rotational quantum number. However, for some vibrational states the linewidth shows a non-monotonic behavior with K, which is the result of mixing with highly excited vibrational levels in the continuum of the ground electronic state. This effect is even more striking, when the total angular momentum quantum number J is varied: In some cases, the linewidth exhibits a pronounced resonancelike behavior as function of J. The agreement with recent experimental spectroscopic data is satisfactory. The calculated linewidths are of the same order (within a factor of 2 or so) as the experimental ones. However, because the two *ab initio* potential energy surfaces do not reproduce sufficiently well the $\tilde{X}$–$\tilde{A}$ excitation energies, the resonancelike effects are not quantitatively described. Potential energy surfaces with considerably higher accuracy are required. © *2001 American Institute of Physics.* [DOI: 10.1063/1.1384456]

I. INTRODUCTION

The predissociation dynamics of vibrational states in the $\tilde{A}\,^1A''$ electronic state of HNO has been studied experimentally by several groups[1–6] (see Ref. 7 for a thorough discussion of the spectroscopy of HNO in the $\tilde{A}$ state). Possible sources for the predissociation mechanism are Renner–Teller (or electronic Coriolis) coupling with the ground electronic state, $\tilde{X}\,^1A'$, and spin–orbit coupling with the lowest triplet state, $\tilde{a}\,^3A''$.

The earliest investigation of lifetime broadening of an absorption line is that of Bancroft *et al.*[1] concerning the (1,0,1)–(0,0,0) transition. (In what follows, v_1, v_2, and v_3 are the number of quanta in the H–N mode, i.e., the dissociation coordinate, the N–O mode, and the bending mode, respectively.) They reported an approximately linear increase in the linewidths from $0.3\,\mathrm{cm}^{-1}$ for transitions to $K=1$ to $0.7\,\mathrm{cm}^{-1}$ for transitions terminating at $K=4$. In what follows, K indicates the projection quantum number of the total angular momentum on the a-axis, essentially the N–O bond. Later, Freedman[2] performed a more detailed and higher-resolution study of the 1–0 sub-band of the same vibronic transition. He observed a pronounced J dependence with the widths reaching a maximum at $J=7$. Moreover, for all values of J considered the widths for $K=0$ were smaller than for $K>0$ and showed the tendency to increase with J.

Recently, Pearson *et al.*[6,7] substantially extended the analysis of lifetime broadening in the $\tilde{A}$ state of HNO. They measured linewidths for a total of six vibronic states above the $\mathrm{H}(^2S)+\mathrm{NO}(X\,^2\Pi)$ dissociation threshold, including the previously studied (1,0,1) state, and various quanta of K. In addition to the increase with K, it was observed that the widths for states with one quantum of bending excitation, (1,0,1) and (1,1,1), are larger than for the corresponding states (1,0,0) and (1,1,0) without bending excitation. These experimental findings point to the Renner–Teller (RT) coupling between the $\tilde{A}\,^1A''$ quasibound states and the continuum states of the $\tilde{X}\,^1A'$ electronic ground state as the primary dissociation mechanism. At linear nuclear configurations the $\tilde{X}$ and the $\tilde{A}$ state of HNO form the two components of a doubly degenerate Δ state (Fig. 1). RT coupling is proportional to K and essentially confined to near linear geometries. As a consequence, the linewidths are expected not only to increase with K but also with v_3 as excitation of the bending mode increases the probability of finding the molecule near the linear geometry. As surmised in Ref. 7 and affirmed below by exact dynamics calculations, the observed strong J dependence of Γ for some of the rovibronic levels arises from tuning into resonance with particular (resonance) states belonging to the $\tilde{X}$ manifold, which are more efficiently coupled to the continuum than the $\tilde{A}$ quasibound states.

In the present article we investigate the RT coupled $\tilde{X}\,^1A'$–$\tilde{A}\,^1A''$ two-surface system in order to gain insight about the predissociation mechanism of the vibrational-

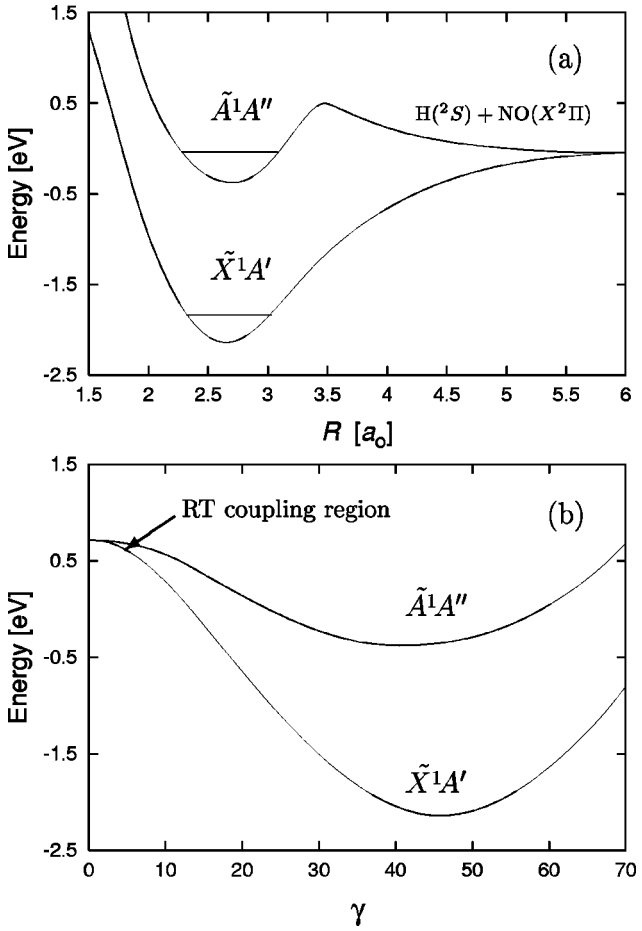

FIG. 1. One-dimensional cuts through the $\tilde{X}\,^1A'$ and $\tilde{A}\,^1A''$ potential energy surfaces along the Jacobi dissociation coordinate R (a) and the Jacobi bending angle γ (b). The potential is minimized in the other two coordinates. $\gamma=0$ corresponds to linear HNO. The horizontal lines in (a) indicate the two zero-point energies.

rotational levels in the upper electronic state from a full dynamics calculation. We will show that most of the experimental results can be—at least qualitatively—explained in terms of this interaction mechanism. Spin–orbit coupling to the triplet state is not taken into account in our study.

The two potential energy surfaces (PES), the Hamiltonian, and the numerical methods are briefly described in Sec. II. The results and their relationship to the available experimental data are discussed in Secs. III and IV, respectively. We will focus the discussion on (i) the rovibrational energies and the rotational constants, (ii) the linewidths and their dependence on the quantum numbers v_1, v_2, v_3, K, and J, and (iii) the mixing with the resonance states in the ground-state manifold. A short discussion and summary completes the article in Sec. V.

II. THEORY

The three-dimensional PESs for the three lowest electronic states—$\tilde{X}\,^1A'$, $\tilde{A}\,^1A''$, and $\tilde{a}\,^3A''$—of HNO have been calculated by *ab initio* methods.[8] All relevant features of the surfaces have been previously discussed in detail. Here, we merely summarize the main characteristics of the RT coupled $\tilde{X}$ and $\tilde{A}$ surfaces. The potential energy surfaces of Guadagnini *et al.*[9] are quite similar to the ones used in the present work. In what follows, energy is measured with respect to the H+NO(r_e) asymptote, if not otherwise stated.

While the ground state PES has a well depth of 2.14 eV with 215 bound states and no barrier to dissociation [Fig. 1(a)], the well of the $\tilde{A}\,^1A''$ excited state is comparably flat (0.38 eV) and dissociation on this surface is hindered by a barrier of 0.50 eV. Thus, the only way by which the low-lying vibrational levels of $\tilde{A}$ can dissociate leads via the electronic ground state. Both surfaces correlate with the same products, that is, ground state NO($X\,^2\Pi$) and H(^2S). The calculated dissociation energy is[8] D_0(H–NO) $=15\,211\,\mathrm{cm}^{-1}$ and agrees well with all previous *ab initio* calculations.[9–12] However, it underestimates the experimental value[13,14] of $16\,450\pm10\,\mathrm{cm}^{-1}$ by $1240\,\mathrm{cm}^{-1}$. Furthermore, the electronic origin of the transition between the $\tilde{A}$ and the $\tilde{X}$ surface is measured[1,15] to be $13\,154\,\mathrm{cm}^{-1}$ while the calculated value is $13\,985\,\mathrm{cm}^{-1}$. As will be seen below, these discrepancies in the dissociation and in the transition energy complicate the quantitative comparison between experiment and theory. Nevertheless, we believe that the calculated surfaces are useful for investigating the overall predissociation mechanism of HNO in an adequate manner, despite the fact that details are not satisfactorily reproduced.

RT coupling is a particular case of the breakdown of the Born–Oppenheimer approximation (see Refs. 16–21 for general discussions and reviews). It is the result of the interaction between the two components of a degenerate electronic state ($\Pi,\Delta,...$). In our previous work on RT coupling in HCO,[22–24] we closely followed the approaches of Petrongolo[25] and Goldfield *et al.*[26] The key is a transformation from adiabatic electronic wave functions to diabatic ones, which—at linear geometries—are eigenfunctions of $\hat{L}_z$, the projection of the electronic angular momentum on the body-fixed z-axis (the C–O bond in HCO or the NO bond in HNO). The corresponding eigenvalues are $\lambda=\pm1$ for a Π molecule (HCO) and ±2 for a Δ molecule (HNO).

The Hamiltonian used in the present investigation for HNO is identical to the Hamiltonian employed in Ref. 24 for studying RT induced decay in HCO. The only difference is that $\lambda=\pm2$ rather than ±1 as for HCO. As a result, the projection quantum l associated with the nuclear angular momentum $\hat{N}_z$ assumes the two values $l=K-\lambda$, with $K=0,\ldots,J$ being the projection quantum number of the total angular momentum (electronic plus nuclear). Except for this difference all equations are the same as in Sec. II A of Ref. 24. For subsequent discussions it is useful to recall that the RT coupling term in the Hamiltonian is proportional to $\hat{J}_z\hat{L}_z/\sin^2\gamma$, where $\hat{J}_z$ is the projection of the total angular momentum on the body-fixed axis. The dynamics calculations are performed in the Jacobi coordinates appropriate for H+NO: R, the distance from H to the center-of-mass of NO, r, the NO bond distance, and γ, the angle between **R** and **r** with $\gamma=0$ corresponding to linear HNO.

The numerical methods, too, are equivalent to those employed for HCO.[24] All dynamics calculations are performed using the filter diagonalization method.[27–29] In a first step,

TABLE I. Energies and rotational constants (in cm^{-1}) of the lowest 21 vibrational states in the $\tilde{A}\,^1A''$ electronic state ($J=K=0$).

(v_1,v_2,v_3)	E (eV)	$E(cm^{-1})$	$E_{expt.}\,(cm^{-1})$[a]	A	B	C
(0,0,0)	−0.025 23[b]	0.0[c]	0.0[c]	21.41	1.31	1.23
(0,0,1)	0.097 04	986.2	981.2	22.72	1.30	1.22
(0,1,0)	0.150 92	1420.8	1420.8	21.06	1.29	1.21
(0,0,2)	0.223 07	2002.6	1959.4	24.64	1.29	1.22
(0,1,1)	0.271 14	2390.3	2389.0	22.44	1.28	1.21
(0,2,0)	0.320 96	2792.2	2801.5	20.26	1.29	1.21
(1,0,0)	0.327 62	2845.9	2854.2	20.08	1.30	1.22
(0,0,3)	0.349 49	3022.3	2932.2	27.09	1.29	1.21
(0,1,2)	0.395 80	3395.8	⋯	24.28	1.27	1.20
(0,2,1)	0.439 58	3748.9	3795.6	21.88	1.28	1.20
(1,0,1)	0.447 45	3812.4	3816.2	21.72	1.30	1.21
(0,0,4)	0.475 81	4041.1	⋯	30.37	1.28	1.21
(0,3,0)	0.489 02	4147.7	4155.4	19.99	1.27	1.19
(1,1,0)	0.501 38	4247.3	4267.7	19.57	1.29	1.20
(0,1,3)	0.521 33	4408.3	⋯	26.69	1.27	1.20
(0,2,2)	0.562 56	4740.8	⋯	23.74	1.27	1.19
(1,0,2)	0.571 08	4809.5	⋯	21.58	1.30	1.20
(0,0,5)	0.601 74	5056.8	⋯	34.89	1.27	1.21
(0,3,1)	0.605 39	5086.3	⋯	21.50	1.26	1.18
(2,0,0)	0.609 04	5115.7	⋯	12.95	1.42	1.21
(1,1,1)	0.619 00	5196.0	5211.4	20.40	1.28	1.20

[a]Experimental transition energies from Refs. 1 and 3.
[b]Energies with respect to the H+NO(r_e) asymptote.
[c]Transition energies with respect to the (0,0,0) vibrational ground state.

optimally adapted basis functions (''window basis functions'') Ψ_i for a narrow energy range are generated by applying the Green's function $\hat{G}^+(E_i)=(E_i-\hat{H}+iW)^{-1}$ as a filtering operator onto an initial wave packet χ,

$$\Psi_i=\mathrm{Im}\,\hat{G}^+(E_i)\chi. \tag{1}$$

Here, iW represents a complex absorbing potential.[30–32] The filtering is efficiently performed by exploiting the Chebychev polynomial expansion of the Green's function.[28,29,33,34] In the subsequent step the spectral information in the narrow energy window $[E_{\min},E_{\max}]$ is extracted by diagonalizing the Hamiltonian in the small set of basis functions Ψ_i.

After many test calculations we have chosen the coordinate ranges $1.5\,a_0\leqslant R\leqslant 9.0\,a_0$ with 80 potential-optimized points,[35] $1.6\,a_0\leqslant r\leqslant 3.6\,a_0$ with 30 potential-optimized points, and $0\leqslant\gamma\leqslant 180°$ with 70 Gauss–Legendre quadrature points.[36] All points of the three dimensional grid with potential energies larger than 1.8 eV are discarded.

The absorbing potential enters the filtering procedure in form of a damping operator $\exp(-\hat{\gamma})$, whose explicit form on a DVR-grid is given by[28,29,34,37]

$$\hat{\gamma}(R)=\frac{D_0}{\sqrt{\Delta H}}\left(\frac{R-R_{\mathrm{damp}}}{R_{\max}-R_{\mathrm{damp}}}\right)^2\Theta(R-R_{\mathrm{damp}}). \tag{2}$$

Here, ΔH and Θ denote the spectral range of the Hamiltonian and the ordinary Heaviside step function, respectively. The three adjustable parameters are the damping strength $D_0=0.03$, the starting point for the absorbing potential, $R_{\mathrm{damp}}=6.5\,a_0$, and the end point of the grid in the dissociation coordinate, $R_{\max}=9.0\,a_0$.

The majority of calculations are carried out in the so-called coupled states (CS) approximation, without inclusion of Coriolis coupling between states with different K quantum numbers.[38] In the CS approximation 35 000 Chebychev iterations are found to ensure convergence. Because the density of states roughly increases linearly with the number of K-blocks included, N_K, the number of Chebychev iterations required for convergence also scales with N_K.

III. RESULTS

A. Bound and quasibound states of HNO($\tilde{A}$)

In Table I we list the calculated energies and rotational constants of the bound and quasibound states in the $\tilde{A}\,^1A''$ electronic state. Quasibound states are states, whose energies are below the barrier in the H+NO exit channel, including the zero-point energy of the two internal modes r and γ, but above the H+NO threshold. The dissociation threshold is calculated as 0.118 eV, which means that all but the two lowest states are in the continuum. The numbers differ slightly from those given in Table III of Ref. 8. The reasons are the different numerical treatments in the two investigations and the inclusion of the electronic angular momentum in the present work, whereas this part of the kinetic energy operator was neglected by Mordaunt *et al.*[8] Assessing the agreement with the experimental transition energies[1,3,5] one has to bear in mind, that the original PES had been slightly scaled. The rotational constants A, B, and C have been calculated from the expectation values of the inverse of the moments of inertia I_A, I_B, and I_C as described in Ref. 8.

The agreement with the experimental transition energies is satisfactory, with the exception of the higher bending excitations (0,0,2) and (0,0,3). The reason for this shortcoming may be the relatively large grid spacing of 20° in the *ab*

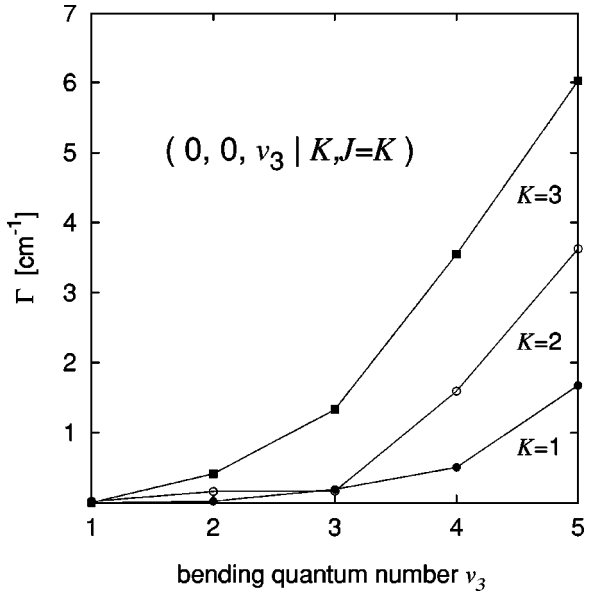

FIG. 2. Linewidths for the pure bending states $(0,0,v_3)_K$. In each case J is identical to K.

initio calculations,[8] which may lead to a not sufficiently accurate description of the PES in the bending coordinate. The two rotational constants B and C differ only slightly and are much smaller than A, i.e., HNO is approximately a prolate top. As expected, A increases strongly with excitation of the bending mode and slightly decreases with excitation of the H–N stretching mode; excitation of the NO stretching mode has little influence on A. The agreement with the measured rotational constants (Table I of Ref. 7) is reasonable; all trends with excitation of the various modes are reproduced. For the subsequent discussion of linewidths it is important to note, that the A rotational constant in the ground electronic state is noticeably smaller than in the $\tilde{A}\,^1A''$ state. For example, $A=18.4\,\mathrm{cm}^{-1}$ for (0,0,0) in the $\tilde{X}$ state. On the other hand, the rotational constants $B=1.40\,\mathrm{cm}^{-1}$ and $C=1.30\,\mathrm{cm}^{-1}$ are slightly larger than their counterparts in the excited state. Thus, by varying K and J one can change the positions of the vibrational states in the $\tilde{A}$ state relative to those in the ground state and thereby modify the mixing between both manifolds and therefore the resonance widths. This effect is very important for HNO and is the main focus in the subsequent discussion.

B. Variation of Γ with bending excitation

HNO is a *bent–bent* RT system, i.e., both electronic states have a nonlinear equilibrium geometry. Thus, as the excitation of the bending mode increases in the excited state, the $\tilde{A}$-state wave function penetrates deeper and deeper into the linear region, where the RT coupling is strongest. As a consequence, the coupling to the ground state and therefore the linewidth Γ strongly increases with v_3 (Fig. 2). The widths for $v_3 \leqslant 1$ and all values of K shown in Fig. 2 are very small: The wave functions have very little overlap with the coupling region near linearity. Incidentally we note, that excitation of the NO stretching mode has only marginal influence on the linewidth. The results for $(0,1,v_3)_{K=5}$, for example, are only marginally different from those for $(0,0,v_3)_{K=5}$. In contrast to HNO, HCO is a *bent–linear* RT system with the upper state being linear. Therefore, increasing the bending quantum number in the excited state pushes the molecule farther and farther away from the linear geometry with the result that—on average—the linewidth decreases with v_3.[22,24,39,40]

Except for $v_3=3$, the K-dependence is monotonic for the particular vibrational states depicted in Fig. 2. That is, however, not universally true, as discussed in what follows.

C. Variation of Γ with *K*

The main part of the RT coupling is proportional to K, the quantum number for the projection of the total angular momentum on the body-fixed z-axis, i.e., essentially the NO axis. As a consequence, following perturbation theory it is expected that the resonance width increases approximately quadratically with K. In order to check this prediction we performed calculations for nine different vibrational states in the $\tilde{A}$ state for $K=J=1$ through 5 (Fig. 3). It is seen, that an approximate K^2 dependence is obtained only for the states (1,0,0), (0,2,1), and (1,0,1), whereas the other six states show a much more complicated and unsystematic behavior.

The rather unpredictable variation of Γ with K reflects the influence of ''resonance'' effects between the quasibound states in the $\tilde{A}$ manifold, on one hand, and the resonance states in the $\tilde{X}$ ground state, on the other. The energy of a prolate top changes with J and K according to

$$E_{J,K}=E_{0,0}+\bar{B}J(J+1)+(A-\bar{B})K^2, \tag{3}$$

where $\bar{B}$ is the average of B and C. Because the rotational constants are different in the two electronic states, changing K or J alters the relative positions of the states in the two manifolds and therefore the interaction between them. The energy variation with K is relatively large and therefore the resonance effects between the two sets of resonance states appear less systematic. The picture becomes much clearer when J is changed for a fixed value of the K quantum number.

D. Variation of Γ with *J*

Since $\bar{B}$ is more than one order of magnitude smaller than A, changing J provides a more favorable means for tuning the energy gap between states in the two electronic states, and thereby the mixing, than variation of K. In Fig. 4 we depict Γ as a function of $J(J+1)$ for the same nine vibrational states as in Fig. 3; $K=3$ in all cases. The RT coupling element does not directly depend on the total angular momentum and therefore perturbation theory predicts that the linewidth should be approximately independent of J. Such a behavior, however, is only seen for the highest vibrational states in Fig. 4. The lower vibrational states, especially (0,1,0) and (0,1,1), show a pronounced resonancelike behavior.

The maxima arise through the mixing with particular resonance states belonging to the ground electronic state, as

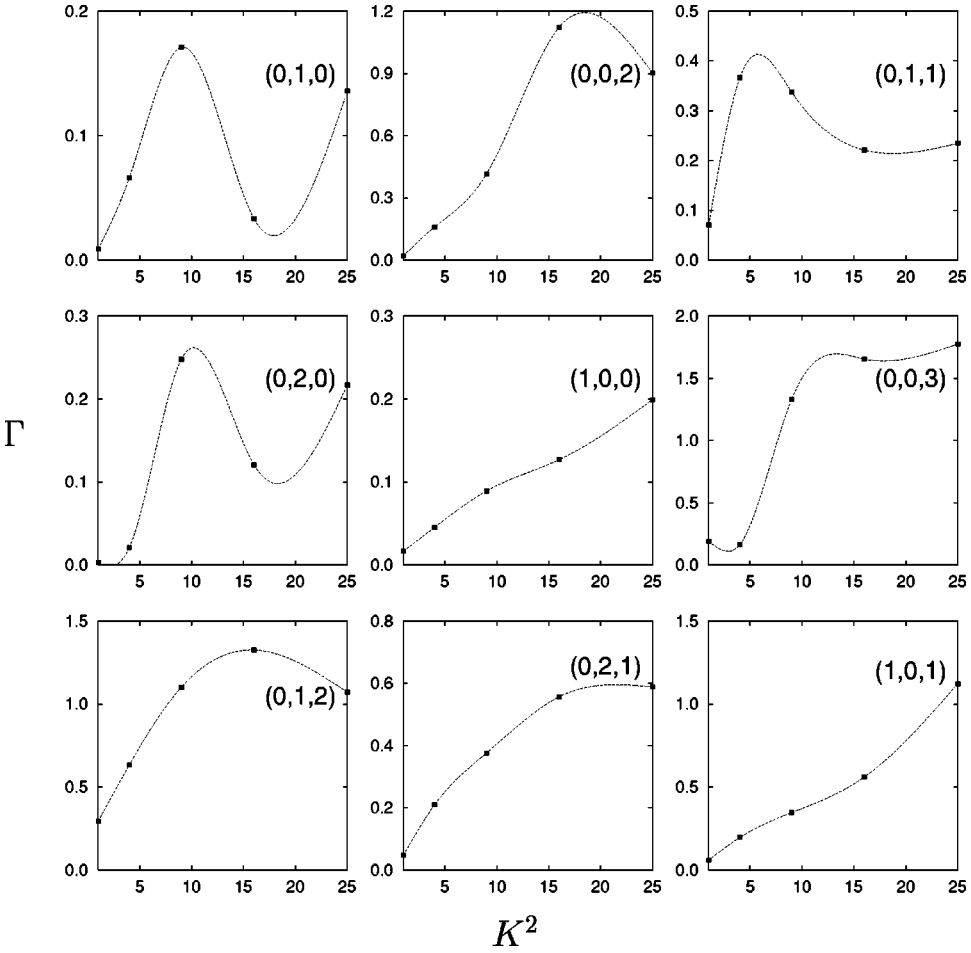

FIG. 3. The variation of the linewidth (cm^{-1}) with the square of the a-axis rotational constant K for nine different vibrational states. In all cases J is identical with K. The smooth lines are intended to guide the eye.

illustrated in more detail in Fig. 5 for (0,1,1) and $K=3$. In the main part of the figure we show Γ versus $J(J+1)$. There are two peaks, a smaller one near $J\sim 11$ and a more pronounced one around $J=21$. The following discussion is focused on the latter maximum. Because of the RT coupling between the two states each wave function has two components—one belonging to the upper state, ψ_A, and one being associated with the ground state, ψ_X. The amplitude of the latter reflects the coupling to the continuum of the ground state. For off-resonance conditions, i.e., when J is far away from the main maximum in Fig. 5, ψ_X is comparably small and has no apparent nodal structure. Changing J does not significantly modify the coupling to the continuum and Γ remains almost constant. However, when (0,1,1) is tuned into resonance with a particular ground-state level, which ''sticks out'' of the continuum in that its wave function is localized in the well region and its width is comparatively small, ψ_X gradually takes on the shape of this particular state; basically, it becomes localized in the potential well of the lower state. This is illustrated in the upper two panels of Fig. 6 showing for $J=21$ the X and A contributions of the (0,1,1) state, i.e., the ''bright state.'' Although the nodal structure of ψ_X is complicated and although an assignment is not apparent, ψ_X for $J\sim 21$ is structurally different from ψ_X for off-resonance conditions.

The change of the wave function across a resonancelike peak reflects the gradual tuning-in and tuning-out of the ''bright'' state (0,1,1) with the perturbing or ''dark'' state, which, because there is no assignment, we will call $(v_1,v_2,v_3)_X$. Important to note is that, although $(v_1,v_2,v_3)_X$ has no clear-cut assignment, it can be recognized as J varies, i.e., its identity is unambiguous. The perturbing state is highly excited in the NO stretching mode; however, the bending mode is certainly excited, too. The wave function of the perturbing state for $J=21$ is also shown in Fig. 6. It has also two contributions, a large one with a nonassignable nodal structure equivalent to $(v_1,v_2,v_3)_X$ and a smaller one with a clear (0,1,1) structure associated with the $\tilde{A}$ state.

The inset of Fig. 5 shows the linewidths for the ''bright'' and the ''dark'' state as functions of the energy mismatch, $\Delta E=E_{(v_1,v_2,v_3)}-E_{(0,1,1)}$. First, the dark state is below the bright one and ΔE is negative. Since $\overline{B}$ of the ground state is larger than $\overline{B}$ in the excited state, the two vibrational states approach each other and around $J=21$ more or less coalesce. Finally, they separate again on the high-J side of the resonance maximum. Because the resonance width for $(v_1,v_2,v_3)_X$ is much larger than the width for state (0,1,1), the latter is drastically increased when $\Delta E\approx 0$. In accord with this behavior, the width of the dark state shows a shallow dip at $J=21$. The half-width of the maximum is $\sim 12\,cm^{-1}$ and thus comparable to the linewidth of the dark state.

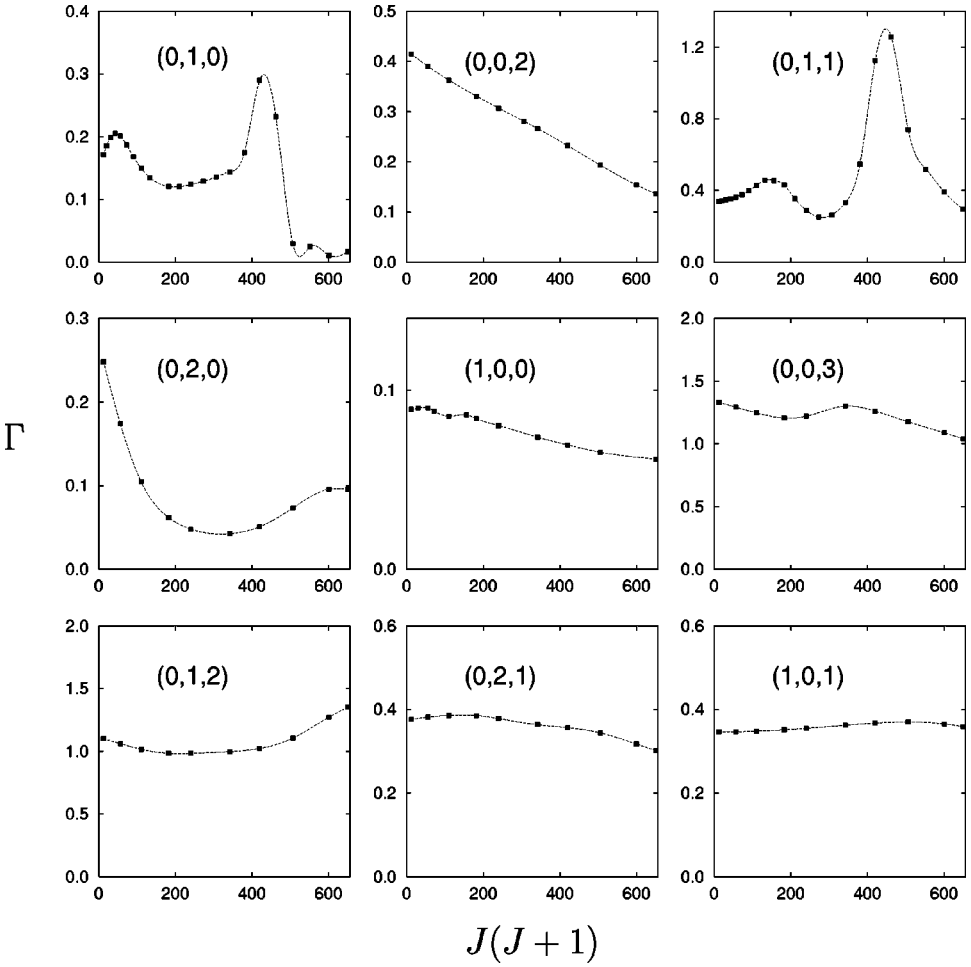

FIG. 4. The variation of the linewidth (cm^{-1}) with $J(J+1)$ for nine different vibrational states. In all cases $K=3$. The smooth lines are intended to guide the eye.

The breadth of the resonancelike structure in Fig. 5 is comparably large, approximately $12\,cm^{-1}$. A considerably narrower structure is depicted in Fig. 7 for state (0,1,0) and $K=2$. The general mechanism is exactly the same as described above for (0,1,1). In this case, however, the width of the perturbing state is only $2-3\,cm^{-1}$; the width of the maximum around $J=12$ is of the same order.

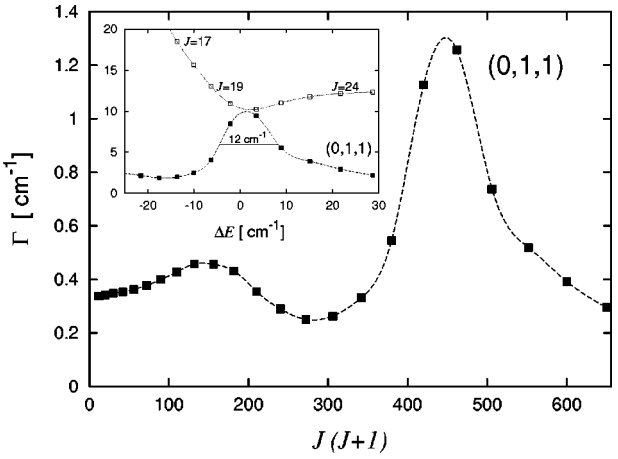

FIG. 5. The linewidth of state (0,1,1) as a function of $J(J+1)$ for $K=3$. The inset shows the width as function of the energy mismatch, ΔE, between the "bright" state (0,1,1) and the "perturbing" state belonging to the ground electronic state. The width of the "bright" state is multiplied by 7.5. See the text for more details.

In order to fully understand the mixing of resonance states belonging to different electronic manifolds, it is important to recall some salient features of the resonance spectrum of the ground electronic state.[41] Up to about 75% of the dissociation energy all bound states can be unambiguously assigned. However, as energy increases the wave functions rapidly become more and more mixed and lose their clear nodal pattern. No continuum state was found with a clear-cut assignment. The states belonging to the pure NO stretching progression can be followed best to high energies, i.e., they retain their identity longest as the energy increases. The degree of irregularity of the resonance states is, however, not so large that a change of the angular momentum from J to $J+1$ in the Hamiltonian markedly changes the appearance of the wave functions. Otherwise, it would not be possible to identify the perturbing state for (0,1,1) and the corresponding resonance width would show a more irregular structure as function of J.

The calculated resonance widths for $J=0$, shown in Fig. 8, fluctuate greatly from state to state. Only states with widths smaller than $30\,cm^{-1}$ are depicted; there are many additional resonances with larger widths. Generally speaking, the smaller the widths the more localized, i.e., confined to the inner part of the potential well are the corresponding

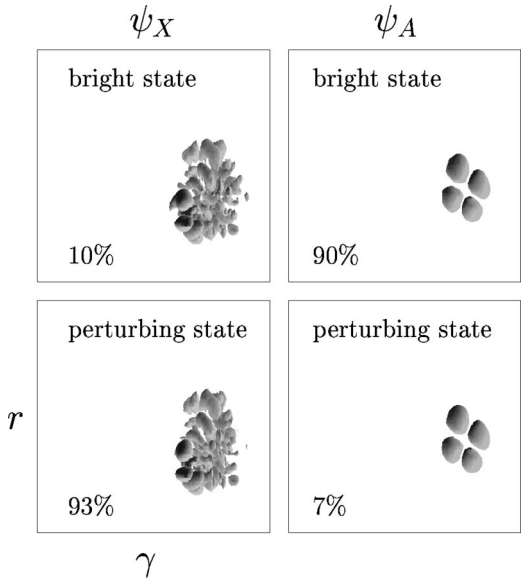

FIG. 6. Upper row: The two wave function contributions ψ_X (left-hand side) and ψ_A (right-hand side) for state (0,1,1). Lower row: The same as in the upper row, but for the perturbing state $(v_1,v_2,v_3)_X$. Shown is the modulus of the wave function. The ordinate is the NO stretching coordinate and the abscissae is the bending angle. The numbers indicate the probabilities with which the two parts contribute to the total wave function. The angular momentum quantum numbers are $K=3$ and $J=21$.

wave functions. The larger the widths the more excited is the dissociation mode and the farther the wave function stretches towards the exit channel. The states with the smallest rates have substantial excitation in the NO stretching coordinate. The states with the very large widths, let us say $\Gamma > 30\,\mathrm{cm}^{-1}$ or so, form the ''continuum'' of the ground electronic state. Because of Franck–Condon arguments, only the states with the smaller widths are believed to perturb the states of the $\tilde{A}$ manifold: The states with high excitation in the dissociation mode naturally have small overlap with the low-excitation states in the $\tilde{A}$ electronic state. The two examples discussed in Figs. 5–7 are prototypes. The missing of

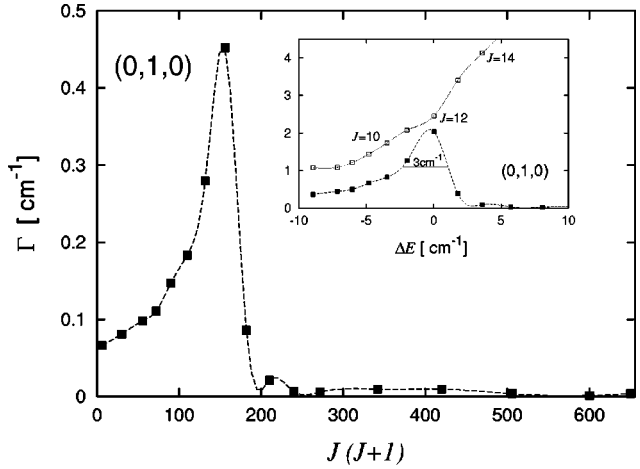

FIG. 7. The linewidth of state (0,1,0) as a function of $J(J+1)$ for $K=2$. The inset shows the width as function of the energy mismatch, ΔE, between the ''bright'' state (0,1,0) and the ''perturbing'' state belonging to the ground electronic state. The width of the ''bright'' state is multiplied by 4.5.

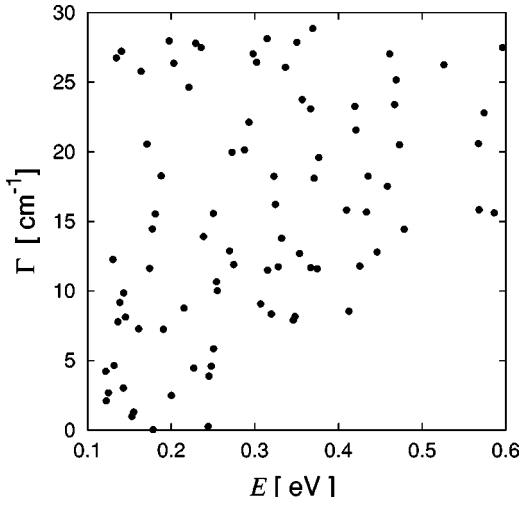

FIG. 8. Calculated widths for the resonance states belonging to the ground electronic state $\tilde{X}$. The total angular momentum is $J=0$. The threshold energy is 0.118 eV.

narrower $\tilde{X}$-state resonances at higher energies may explain, why the widths for the higher $\tilde{A}$-state vibrational states in Fig. 4 have a smoother behavior as a function of J.

The location of the resonancelike structures on the J and K axes depends sensitively on the positions of the levels in the $\tilde{A}$ state relative to the states in the ground state manifold. Because the PESs used in the present investigation do not have the required accuracy, it cannot be expected to reproduce the resonance structures observed in the spectroscopy experiment in a quantitative manner. Nevertheless, the agreement between our calculated linewidths and the observed ones is satisfying, except for the resonance structures.

IV. COMPARISON WITH EXPERIMENTAL LINEWIDTHS

In this section we compare our theoretical results with the linewidths measured by Pearson *et al.*[6,7] for six vibrational states of HNO($\tilde{A}\,^1A''$).

A. (1,0,1)

The (1,0,1) state not only was the first one, for which predissociation had been detected, but it also is the level, for which most measurements have been performed.[1,2,7] The first experimental estimate came from Bancroft *et al.*[1] who found that the linewidth approximately increases linearly with K, from $0.3\,\mathrm{cm}^{-1}$ for $K=1$ to $0.7\,\mathrm{cm}^{-1}$ for $K=4$. The corresponding calculated results (obtained in the CS approximation) are 0.06, 0.20, 0.35, and $0.56\,\mathrm{cm}^{-1}$ for $K=1-4$. The general trend is well reproduced, but our widths are somewhat smaller than the measured ones. The newer measurements of Freedman[2] and Pearson *et al.*[6,7] suggest a J-averaged value of $0.1\,\mathrm{cm}^{-1}$ for $K=1$ which is in better accord with our calculation.

The detailed J-dependence of the width for $K=1$ is illustrated in Fig. 9. The measured widths of Pearson *et al.* for the f-parity [parity is given by $P=(-1)^{J+1}$] show a resonancelike behavior with a maximum at $J=7$. The results of Freedman show a similar trend, but a slightly higher value of

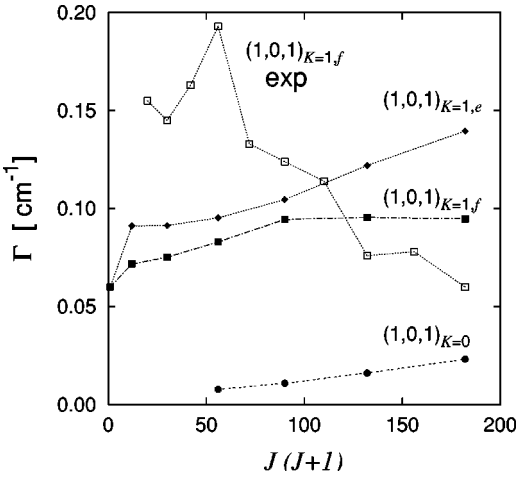

FIG. 9. Comparison of calculated (closed symbols) and measured (open squares, Ref. 7) linewidths for vibrational state (1,0,1) and $K=1$. The parity is given by e and f. For comparison, also the theoretical widths for $K=0$ are shown. See the text for more details.

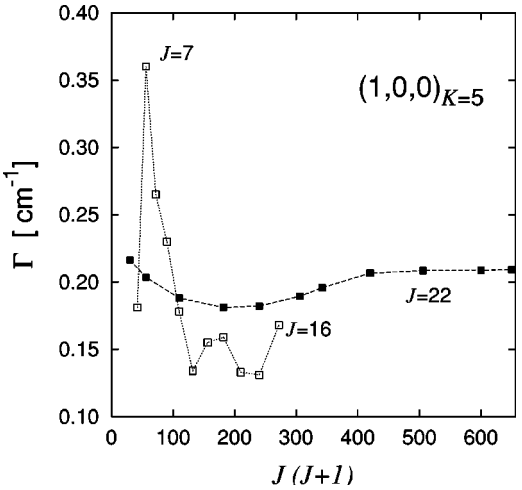

FIG. 10. Comparison of calculated (filled squares) and measured (open squares) widths for vibrational state (1,0,0) and $K=5$.

$0.11\,\mathrm{cm}^{-1}$ for large J quantum numbers. The corresponding theoretical widths for the f-parity are of the same size except for the maximum around $J=7$. These calculations for a definite parity are performed with Coriolis coupling taken into account by including, in addition to $K=1$, also $K=0$ and 2. In this case, the CS approximation, which does not discriminate different parity states, is not sufficiently accurate; the CS width is almost independent of J and noticeably smaller than the more exact result ($0.06\,\mathrm{cm}^{-1}$ for $J=1$ and $0.055\,\mathrm{cm}^{-1}$ for $J=13$).

For completeness we also calculated the widths for the e-parity block $[P=(-1)^J]$. K states from $K=1$ to 3 are included in the calculations; $K=0$ does not exist for the e-parity. Taking into account a fourth K state does not noticeably alter the width. Unfortunately, linewidths for the e-parity block could not be measured—only the line positions up to $J=11$ have been determined. In Table II we compare the theoretical and the experimental energy differences between successive odd J levels. (The even J values have not been calculated.) The agreement is very good showing that the rotational structure of HNO in the excited state is well described by the calculations.

For comparison we show in Fig. 9 also the results for $K=0$. They are generally smaller than the $K=1$ widths. The RT coupling term in the Hamiltonian is proportional to K and therefore vanishes for $K=0$. Transitions to the ground state thus can occur only via mixing with $K>0$ states caused by Coriolis coupling as has been discussed in detail for HCO, for example, by Weiß *et al.*[24] As a consequence, the $K=0$ widths are considerably smaller than the $K=1$ widths. The results for (1,0,1) show an almost linear dependence on $J(J+1)$, which has to be compared to a $J^2(J+1)^2$ dependence for HCO (Fig. 4 in Ref. 24). HNO is bent in the upper state and therefore Coriolis induced $\Delta K=\pm 1$ transitions without changing the vibrational structure are possible. The situation is different for HCO, where the upper state is linear. For a linear molecule symmetry requires that the bending quantum number is even (odd) for odd (even) K quantum numbers. Therefore, a $\Delta K=\pm 1$ transition requires to change the vibrational structure and is therefore much less probable than a $\Delta K=\pm 2$ transition, which does not necessitate a change of v_3. Since Coriolis coupling is proportional to $[J(J+1)]^{1/2}$, the linewidth depends linearly on $J(J+1)$ for HNO and quadratically for HCO.

TABLE II. Comparison of calculated and measured energy differences (in cm^{-1}) between successive *ungerade* J levels of state (1,0,1) for $K=1$ and parity e.

J	$\Delta_{\mathrm{calc.}}$	$\Delta_{\mathrm{expt.}}$
1	12.74[a]	13.10[b]
3	23.26	23.41
5	33.76	33.80
7	44.27	44.21
9	54.87	53.64
11	65.54	⋯

[a] $E_{J'}-E_J$ with $J'=J+2$.
[b] From Table IX of Ref. 7.

B. (1,0,0) and (0,2,0)

The measured linewidths for state (1,0,0) and $K=5$ show a pronounced resonancelike peak at $J=7$ (Fig. 10). The corresponding calculated width does not exhibit any strong variation with J. However, the average experimental value is well reproduced. This is another example where our calculations are on the average in satisfactory agreement with the measurement except for the resonance structure, which depends sensitively on the relative positions of vibrational states in the upper and the lower electronic states.

In the case of (0,2,0) $K=5$ Pearson *et al.*[7] were able to measure decay widths only for three values of J: 7, 9, and 10. They reported an average Lorentzian width of $0.104 \pm 0.012\,\mathrm{cm}^{-1}$ with no pronounced variation with J. The calculated width smoothly decreases from $0.20\,\mathrm{cm}^{-1}$ for $J=5$ to $0.125\,\mathrm{cm}^{-1}$ for $J=25$. Thus, the calculated width reproduces the experimental one within a factor of 2 or so.

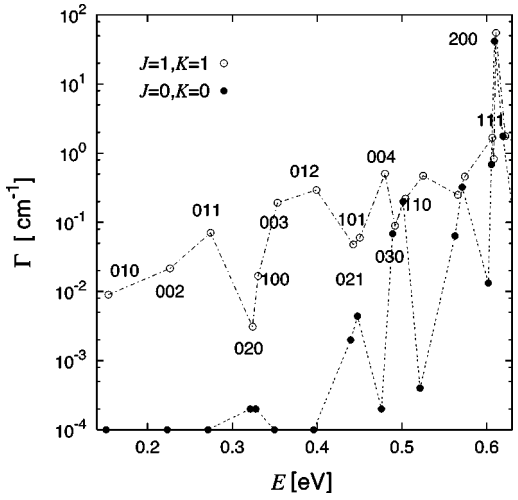

FIG. 11. Comparison of the linewidths for the vibrational states in the $\tilde{A}\,^1A''$ electronic state for $J=K=0$ (filled circles) and $J=K=1$ (open circles).

C. (0,3,0), (1,1,0), and (1,1,1)

Pearson *et al.*[7] have also measured linewidths for the states (0,3,0), (1,1,0), and (1,1,1). Calculations for $J=0$, i.e., without any RT coupling to the $\tilde{X}$ state show that these states already dissociate with appreciable probability on the upper electronic PES as illustrated in Fig. 11. Comparing the $J=0$ calculations with those for $J=K=1$ definitely proves that all states below (0,3,0) primarily dissociate via RT coupling. However, the contribution of RT coupling is much weaker for all states above (0,3,0), with the exception of states with large excitation of the bending mode like (0,1,3) and (0,0,5), for example. The latter are not excited in the dissociation coordinate and therefore have relatively small widths for $J=0$. Switching on Coriolis coupling significantly increases their widths.

State (1,1,1) is already 0.117 eV above the barrier and has a linewidth of $2\,\mathrm{cm}^{-1}$ for $J=0$, which, as we will see below, is much too large compared to the experimental width. This indicates that the dissociation barrier of our PES is too small. In order to correct this shortcoming we artificially increased the barrier by 0.3 eV by adding a Gaussian barrier. This modification ensures that the states (0,3,0), (1,1,0), and (1,1,1) primarily dissociation via RT coupling to the ground states rather than on the excited state. The increase by 0.3 eV is not the result of extensive test calculations and comparisons with the experimental data. It is merely a rough guess. The decay rates of the lower states are not significantly altered by this modification.

For (0,3,0) the only available linewidth is $0.069 \pm 0.011\,\mathrm{cm}^{-1}$ for $J=K=6$. Our calculations with the artificially modified PES yield a smoothly decreasing function with $0.296\,\mathrm{cm}^{-1}$ for $J=6$ and $0.092\,\mathrm{cm}^{-1}$ for $J=20$. The decrease by a factor of 3 indicates that in the calculations strong mixing with a quasibound state in the $\tilde{X}$ state is present for small values of J. The value for large J quantum numbers, far away from the resonance, agrees reasonably well with the experimental value of $0.069\,\mathrm{cm}^{-1}$.

For state (1,1,0) Pearson *et al.*[7] measured linewidths for $K=4-6$. For $K=4$ the decay width smoothly increases to $0.133\,\mathrm{cm}^{-1}$ for $J=16$ with the tendency to reach a slightly higher asymptotic value for larger J states. In the calculations we obtain a value of $0.17\,\mathrm{cm}^{-1}$ almost independent of J. For $K=5$ and 6 only weak J dependencies were observed in the experiment with average widths of $0.156\,\mathrm{cm}^{-1}$ for $K=5$ and $0.169\,\mathrm{cm}^{-1}$ for $K=6$. The calculated widths, too, show only a weak J dependence. However, the average widths, $\sim 0.44\,\mathrm{cm}^{-1}$ and $\sim 0.30\,\mathrm{cm}^{-1}$, are by factors of roughly 3 and 2, too large. Neither the measured nor the calculated rates show the K^2 dependence expected from perturbation theory.

TABLE III. Comparison of calculated and measured linewidths (in cm^{-1}) for the vibrational state (1,1,1) and $K=0$ and 1.

	$K=0$		$K=1$	
J	$\Gamma_{\mathrm{calc.}}$	$\Gamma_{\mathrm{expt.}}$	$\Gamma_{\mathrm{calc.}}$	$\Gamma_{\mathrm{expt.}}$
5	0.014	0.036[a]	0.059	0.052[a]
8	0.018	0.030	0.069	0.086
10	0.027	0.045	0.076	0.090

[a]From Table VI of Ref. 7.

Finally, we consider state (1,1,1) for which widths have been measured for $K=0$ and 1. Pearson *et al.*[7] reported average linewidths of $0.038\,\mathrm{cm}^{-1}$ for $K=0$ and $0.075\,\mathrm{cm}^{-1}$ for $K=1$. If state (1,1,1) were above the dissociation barrier, a much larger width would be expected because of the direct excitation of the dissociation mode (see Fig. 11). The small width of less than a tenth of a cm^{-1} clearly proves that this state is below the dissociation barrier and that the barrier of our original PES is too small. Because of the smallness of the widths it is mandatory to include Coriolis coupling. In all calculations the K-blocks $K=1-2$ are taken into account. The results for $J=5$, 8, and 10 are listed and compared with the experimental data in Table III. In view of the smallness of the widths the agreement is quite good, especially for $K=1$. In the calculations, state (1,1,1) is well below the barrier and the main route for dissociation is undoubtedly via the ground electronic state.

The experimental widths for $K=0$ are considerably smaller than analogous widths for HCO. For example, the $K=0$ width for (0,9,0) in HCO is larger than $0.2\,\mathrm{cm}^{-1}$ (in the upper state of HCO v_3 is the bending quantum number).[42] In Ref. 24 we argued that this relatively large value for $K=0$ is primarily due to the spin–orbit coupling with the ground electronic state rather than RT coupling; the electronic states involved are doublet states for HCO. The corresponding states for HNO are singlet states and spin–orbit coupling is absent.

V. DISCUSSION AND SUMMARY

We have presented a detailed theoretical investigation of the predissociation of HNO in the $\tilde{A}\,^1A''$ electronic state by means of quantum mechanical dynamics calculations including the RT coupling to the ground electronic state $\tilde{X}\,^1A'$. The two corresponding potential energy surfaces had been previously determined by *ab initio* electronic structure calcula-

tions. All three degrees of freedom have been taken into account. The resonance widths of the quasibound states have been calculated by the filter diagonalization method and a complex absorbing potential in the exit channel.

The focus of our investigation was the vibrational and rotational state dependence of the line width (i.e., resonance width) Γ and the comparison of Γ with available experimental data, primarily those of Pearson *et al.*[7] The agreement with the measured widths is generally good: The average theoretical width reproduces the average experimental width within a factor of 2 or so—for many vibrational rotational states. This indicates, that, first, the calculated potential energy surfaces are realistic, and second, that Renner–Tenner coupling is the primary predissociation mechanism.

Finer details, i.e., resonance effects due to mixing with long-lived quasibound states belonging to the ground vibrational state are not quantitatively reproduced. Resonance induced maxima in the J dependence of Γ do exist, but not for the right J values. These discrepancies are not surprising because a quantitative description requires potential energy surfaces, which are significantly more accurate than the ones used in the present work. The dissociation energy of the ground state and, probably more importantly, the vertical excitation energy should be accurate to at least a few tens of a cm^{-1}. In addition to the unprecise dissociation and vertical excitation energy, the dissociation barrier in the excited state is too low by about 0.3 eV.

The mixing between quasibound states belonging to different electronic states is an interesting effect. A quasibound state in the upper electronic manifold is coupled, via nonadiabatic coupling, to the continuum of the ground electronic state and simultaneously it is coupled to another quasibound state, which belongs to the $\tilde{X}$-state continuum. In the nuclear physics literature the latter is called ''doorway state.'' A simple model based on Fano's theory of autoionization[43] has been derived by Ashfold *et al.*[44] to describe predissociation in NO. In our calculations the continuum can be thought of being the overlap of many broad resonances as illustrated in Fig. 8. As the energy mismatch of the two quasibound states decreases, for example, by changing the rotational quantum number, the mixing increases and the widths of the two states, as well as other spectroscopic constants, show relatively sharp changes. In the examples discussed in the present investigation the widths of the two states are considerably different. This is a special situation. However, what happens if the two coupled states have similar widths? Another interesting question is, which of the many resonance states in the ground-state manifold can serve as a doorway state? According to the (limited) experience made in our HNO study we think that the mixing can occur only with the narrower resonance states, those which are confined to the same spatial region. The broader resonances are more delocalized on the ground-state potential energy surface and the Franck–Condon factors with the well confined states in the upper state are unfavorable. Actually, the mixing with the broad resonances constitutes the coupling to the ''continuum.'' In view of Fig. 6 it is astonishing that wave functions with so different nodal structures can lead to pronounced resonance effects.

Resonance induced variations of resonance widths have also been observed in other polyatomic molecules, for example the dissociation of HOCl in its ground electronic state.[45–48] Monitoring the decay width for vibrational state (6,0,0) (v_1 is the HO vibrational quantum number) as a function of J shows several fluctuations, which qualitatively can be explained in an analogous way as described for the HNO predissociation. In an adiabatic picture, in which the fast HO mode is decoupled from the other two modes, the unimolecular dissociation of HOCl can be viewed as a multistate problem. The mixing then occurs between states belonging to different v_1-manifolds, rather than different electronic states. Since the density of states is much higher for HOCl than for HNO, the resonance effects have a more unsystematic appearance.

Resonances between resonance states are common features in molecular physics and deserve a more thorough theoretical investigation.

ACKNOWLEDGMENTS

The authors gratefully acknowledge financial support by the Deutsche Forschungsgemeinschaft within the Sonderforschungsbereich 357 ''Molekulare Mechanismen Unimolekularer Reaktionen'' and by the Fonds der Chemischen Industrie. They are indebted to S. Yu. Grebenshchikov for stimulating discussions.

[1] J. L. Bancroft, J. M. Hollas, and D. A. Ramsay, Can. J. Phys. **40**, 322 (1962).
[2] P. A. Freedman, Chem. Phys. Lett. **44**, 605 (1976).
[3] R. N. Dixon, K. B. Jones, M. Noble, and S. Carter, Mol. Phys. **42**, 455 (1981).
[4] R. N. Dixon, M. Noble, C. A. Taylor, and M. Delhoume, Faraday Discuss. Chem. Soc. **71**, 125 (1981).
[5] R. N. Dixon and C. A. Rosser, J. Mol. Spectrosc. **110**, 262 (1985).
[6] J. Pearson, A. J. Orr-Ewing, M. N. R. Ashfold, and R. N. Dixon, J. Chem. Soc., Faraday Trans. **92**, 1283 (1996).
[7] J. Pearson, A. J. Orr-Ewing, M. N. R. Ashfold, and R. N. Dixon, J. Chem. Phys. **106**, 5850 (1997).
[8] H. D. Mordaunt, H. Flöthmann, M. Stumpf, H.-M. Keller, C. Beck, R. Schinke, and K. Yamashita, J. Chem. Phys. **107**, 6603 (1997).
[9] R. Guadagnini, G. C. Schatz, and S. P. Walch, J. Chem. Phys. **102**, 774 (1995).
[10] F. Pauzat, Y. Ellinger, G. Berthier, M. Gerin, and Y. Viala, Chem. Phys. **174**, 71 (1991).
[11] O. Nomura, Int. J. Quantum Chem. **18**, 143 (1980).
[12] S. P. Walch and C. M. Rohlfing, J. Chem. Phys. **91**, 2939 (1989).
[13] R. N. Dixon, K. B. Jones, and M. Noble, Mol. Phys. **42**, 455 (1980).
[14] R. N. Dixon, J. Chem. Phys. **104**, 6905 (1996).
[15] F. W. Dalby, Can. J. Phys. **40**, 322 (1958).
[16] G. Herzberg, *Molecular Spectra and Molecular Structure III. Electronic Spectra and Electronic Structure of Polyatomic Molecules* (Van Nostrand, Princeton, 1967).
[17] G. Duxbury, Chem. Soc. Spec. Per. Rep. Mol. Spectrosc. **3**, 497 (1975).
[18] P. R. Bunker, *Molecular Symmetry and Spectroscopy* (Academic, San Diego, 1979).
[19] M. Perić, S. D. Peyerimhoff, and R. J. Buenker, Int. Rev. Phys. Chem. **4**, 85 (1985).
[20] J. M. Brown and F. Jørgensen, Adv. Chem. Phys. **52**, 117 (1982).
[21] S. Carter, N. C. Handy, P. Rosmus, and G. Chambaud, Mol. Phys. **71**, 605 (1990).
[22] A. Loettgers, A. Untch, H.-M Keller, R. Schinke, H.-J. Werner, C. Bauer, and P. Rosmus, J. Chem. Phys. **106**, 3186 (1997).
[23] A. Loettgers and R. Schinke, J. Chem. Phys. **106**, 8938 (1997).
[24] J. Weiß, R. Schinke, and V. A. Mandelshtam, J. Chem. Phys. **113**, 4588 (2000).

[25] C. Petrongolo, J. Chem. Phys. **89**, 1297 (1988).
[26] E. M. Goldfield, S. K. Gray, and L. B. Harding, J. Chem. Phys. **99**, 5812 (1993).
[27] M. R. Wall and D. Neuhauser, J. Chem. Phys. **102**, 8011 (1995).
[28] V. A. Mandelshtam and H. S. Taylor, J. Chem. Phys. **102**, 7390 (1995).
[29] T. P. Grozdanov, V. A. Mandelshtam, and H. S. Taylor, J. Chem. Phys. **103**, 7990 (1995).
[30] G. Jolicard and E. J. Austin, Chem. Phys. Lett. **121**, 106 (1985).
[31] G. Jolicard and E. J. Austin, Chem. Phys. **103**, 295 (1986).
[32] U. V. Riss and H.-D. Meyer, J. Phys. B **24**, 4503 (1993).
[33] R. Kosloff, Annu. Rev. Phys. Chem. **45**, 145 (1994).
[34] V. A. Mandelshtam, T. P. Grozdanov, and H. S. Taylor, J. Chem. Phys. **103**, 10074 (1995).
[35] J. Echave and D. C. Clary, Chem. Phys. Lett. **190**, 225 (1992).
[36] Z. Bačić and J. C. Light, Annu. Rev. Phys. Chem. **40**, 469 (1989).
[37] V. A. Mandelshtam and H. S. Taylor, J. Chem. Soc., Faraday Trans. **93**, 847 (1997).
[38] F. A. Gianturco, *The Transfer of Molecular Energy by Collisions* (Springer, Heidelberg, 1979).
[39] D. W. Neyer, S. H. Kable, J.-C. Loison, P. L. Houston, I. Burak, and E. M. Goldfield, J. Chem. Phys. **97**, 9036 (1992).
[40] R. N. Dixon, Mol. Phys. **54**, 333 (1985).
[41] R. Schinke, C. Beck, S. Yu. Grebenshchikov, and H.-M. Keller, Ber. Bunsenges. Phys. Chem. **102**, 593 (1998).
[42] R. Vasudev and R. N. Zare, J. Chem. Phys. **76**, 5267 (1982).
[43] U. Fano, Phys. Rev. **124**, 1866 (1961).
[44] M. N. R. Ashfold, R. N. Dixon, J. D. Prince, B. Tutcher, and C. M. Western, J. Chem. Soc., Faraday Trans. 2 **82**, 1257 (1986).
[45] A. Callegari, J. Rebstein, R. Jost, and T. R. Rizzo, J. Chem. Phys. **111**, 7359 (1999).
[46] G. Dutton, R. J. Barnes, and A. Sinha, J. Chem. Phys. **111**, 4976 (1999).
[47] S. Skokov and J. M. Bowman, J. Chem. Phys. **110**, 9789 (1999).
[48] J. Hauschildt, J. Weiß, and R. Schinke, Z. Phys. Chem. (Munich) **214**, 609 (2000).